ACS Chemical Neuroscience

Research Article

pubs.acs.org/chemneuro

In Situ Biospectroscopic Investigation of Rapid Ischemic and Postmortem Induced Biochemical Alterations in the Rat Brain

Mark J. Hackett,[†] Carter J. Britz,[§] Phyllis G. Paterson,[‡] Helen Nichol,[§] Ingrid J. Pickering,[†] and Graham N. George*[,†]

[†]Molecular and Environmental Sciences Group, Department of Geological Sciences, University of Saskatchewan, 114 Science Place, Saskatoon, Saskatchewan S7N 5E2, Canada

[‡]College of Pharmacy and Nutrition, University of Saskatchewan, D Wing Health Sciences, 107 Wiggins Road, Saskatoon, Saskatchewan S7N 5E5, Canada

[§]Department of Anatomy and Cell Biology, University of Saskatchewan, 107 Wiggins Rd, Saskatoon, Saskatchewan S7N 5E5, Canada

Supporting Information

ABSTRACT: Rapid advances in imaging technologies have pushed novel spectroscopic modalities such as Fourier transform infrared spectroscopy (FTIR) and X-ray absorption spectroscopy (XAS) at the sulfur K-edge to the forefront of direct in situ investigation of brain biochemistry. However, few studies have examined the extent to which sample preparation artifacts confound results. Previous investigations using traditional analyses, such as tissue dissection, homogenization, and biochemical assay, conducted extensive research to identify biochemical alterations that occur ex vivo during sample preparation. In particular, altered metabolism and oxidative stress may be caused by animal death. These processes were a concern for studies using biochemical assays, and protocols were developed to minimize their occurrence. In this investigation, a similar approach was taken to identify the biochemical alterations that are detectable by two in situ spectroscopic methods (FTIR, XAS) that occur as a consequence of ischemic conditions created during humane animal killing. FTIR and XAS are well suited to study markers of altered metabolism such as lactate and creatine (FTIR) and markers of oxidative stress such as aggregated proteins (FTIR) and altered thiol redox (XAS). The results are in accordance with previous investigations using biochemical assays and demonstrate that the time between animal death and tissue dissection results in ischemic conditions that alter brain metabolism and initiate oxidative stress. Therefore, future in situ biospectroscopic investigations utilizing FTIR and XAS must take into consideration that brain tissue dissected from a healthy animal does not truly reflect the in vivo condition, but rather reflects a state of mild ischemia. If studies require the levels of metabolites (lactate, creatine) and markers of oxidative stress (thiol redox) to be preserved as close as possible to the in vivo condition, then rapid freezing of brain tissue via decapitation into liquid nitrogen, followed by chiseling the brain out at dry ice temperatures is required.

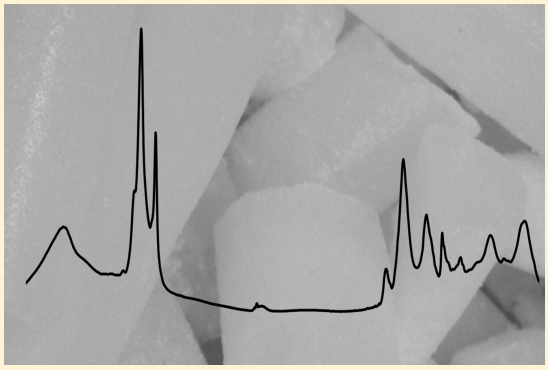

KEYWORDS: *XAS, FTIR, ischemia, metabolism, oxidative stress, neuroscience*

The huge human and economic cost of neurodegenerative diseases worldwide drives research into improved therapies based on a more complete understanding of the biochemical mechanisms underlying neuronal cell death. Unfortunately, even the best microscopic techniques do not provide a detailed biochemical picture, and biochemical assays like nuclear magnetic resonance (NMR) or mass spectroscopy generally lack the spatial resolution needed to link biochemical changes with structural pathology. However, the combination of synchrotron X-ray absorption spectroscopy (XAS),[1−4] X-ray fluorescence spectroscopy,[5−18] and Fourier transform infrared spectroscopy (FTIR)[10,19−31] to analyze cells in situ can localize a wide range of biochemical parameters with cellular or subcellular spatial resolution.

A significant obstacle in the progression of studies in this field has been the use of inappropriate sample preparation methods, resulting in removal of important biochemical information or the introduction of chemical artifacts.[1,32] The imaging capabilities available for in situ spectroscopic methods using synchrotron light inherently imply that sample preparation must preserve both cell morphology and biochemistry. This is in contrast to traditional methods used in the neuroscience field that require either preservation of morphology or preservation of biochemistry, but not both.

Received: July 19, 2014
Revised: October 9, 2014
Published: October 28, 2014

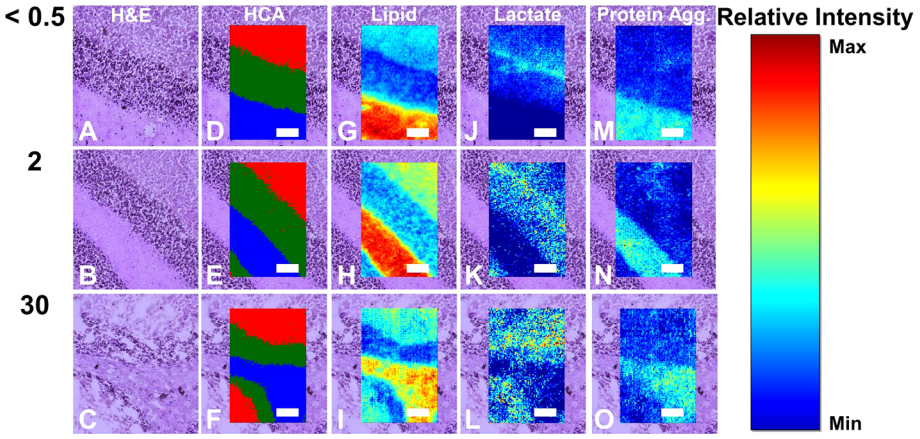

Figure 1. FTIR spectroscopic imaging of cerebellum prepared by (A, D, G, J, M) method A, <0.5 min after animal death; (B, E, H, K, N) method B, 2 min after animal death; (C, F, I, L, O) method C, 30 min after animal death. (A–C) H&E histology. (D–F) Three group cluster image from HCA analysis of second-derivative spectra (1490–1000 cm^{-1}). Red = molecular layer, green = granular layer (gray matter), blue = inner white matter. (G–I) The relative lipid distribution generated from second-derivative intensity at 1742 cm^{-1}. (J–L) The relative lactate distribution generated from second-derivative intensity at 1127 cm^{-1}. (M–O) The relative aggregated protein distribution generated from second-derivative intensity at 1625 cm^{-1}. Scale bar = 50 μm. Relative intensity scale refers to the lipid, lactate, and aggregated protein images.

It is well established that rapid cryo-preservation of brain tissue such as freeze-blowing, whole body immersion into liquid nitrogen, or decapitation into liquid nitrogen is required for bulk quantitative assay of metabolites and antioxidants at levels as close as possible to those present in vivo. Failure to rapidly cryo-preserve brain tissue results in significant alterations in the levels of many key biochemical compounds during the postmortem interval (PMI) due to ischemic conditions created by disrupted blood flow at the time of death, autolytic processes occurring after death, or oxidation of the tissue in air during tissue dissection.[33−42] The biochemical responses of the brain to disrupted blood flow, lack of oxygen, and energy supply begin within seconds and often peak and plateau within several minutes.[33−42] Therefore, biochemical differences between brain regions or animal groups (i.e., "healthy" and "diseased") that were present in vivo may be lost.

The XAS, X-ray fluorescence, and FTIR biological spectroscopic communities have been slow to adopt protocols for the rapid in situ flash freezing of the brain that are common practice for quantitative analytical biochemical analysis of the brain, such as freezing the brain within the skull. Many biochemical imaging studies use formalin-fixed tissue or brain tissue that is dissected first and then flash frozen. While it has been shown that the latter is superior to the former in preserving the in vivo biochemistry,[1,32] the time period for tissue dissection (1–3 min) may still result in significant biochemical alterations within the brain relative to the in vivo state. Therefore, an analytical hypothesis-driven approach is essential for biological spectroscopic studies of brain tissue, with careful consideration of the biochemical alterations that are likely to occur during all stages of sample preparation.

In this study we have performed the first detailed in situ biospectroscopic investigation of the biochemical alterations that occur following animal death. We compare biochemical variations in the cerebellum of healthy untreated rats due to preparation by three different methods: (A) decapitation into liquid nitrogen (<0.5 min PMI), (B) brain dissection followed by rapid flash freezing (2 min PMI), or (C) tissue dissection and delayed flash freezing of brain tissue (30 min PMI). We focus on alterations in the relative levels of four important biochemical parameters: (1) lactate (studied by FTIR), (2) protein aggregates (studied by FTIR), (3) phosphocreatine/creatine equilibrium (studied by FTIR), and (4) thiol redox status (studied by XAS at the sulfur K-edge). These four biochemical parameters were chosen because they have previously been extensively investigated in tissue homogenates using biochemical assays, alterations in their concentration within the postmortem interval are well characterized at the bulk tissue level, and these parameters are widely used as markers of various neurological disease states. We show that even a short PMI results in changes to lactate, phosphocreatine/creatine equilibrium, and thiol/disulfide ratios that are detectable by FTIR and XAS. In addition, we have observed for the first time a rapid decrease in thioether content of brain tissue in response to ischemia induced by animal death. Since the model we use is the most simple and earliest model of brain ischemia without reperfusion, our findings have important methodological implications for studying ischemic stroke. We note that although FTIR spectroscopic imaging was performed in this study, XAS at the sulfur K-edge was not used in an imaging modality, but rather for in situ bulk measurement of the average sulfur speciation. Nonetheless, this study highlights the potential of this multimodal biospectroscopic approach incorporating FTIR and XAS at the sulfur K-edge for future investigation of cerebral ischemia using more elegant preclinical stroke models that more closely resemble clinical stroke.

RESULTS AND DISCUSSION

Preparation of Brain Tissue. Brains from healthy rats were prepared by one of the following three methods that incorporate different postmortem intervals (PMI), as fully described in Methods: (A) decapitation into liquid nitrogen (<0.5 min PMI); (B) decapitation and removal of the brain followed by rapid flash freezing (2 min PMI); (C) decapitation as in (B) but followed by a delay of 30 min before flash freezing (30 min PMI).

Histology. Following spectroscopic analyses, tissue sections were fixed in formaldehyde gas followed by staining with hematoxylin and eosin (H&E). Cell and tissue structure of the cerebellum prepared by each of the three methods, <0.5 min (method A), 2 min (method B) or 30 min (method C), is shown in the histology images presented in Figure 1A–C.

dx.doi.org/10.1021/cn500157j | ACS Chem. Neurosci. 2015, 6, 226–238

Cerebellum tissue prepared after a 30 min PMI (method C) displayed significant edema and tissue damage, relative to tissue prepared after a PMI of <0.5 or 2 min (method A or B, respectively). Histology of tissue prepared after <0.5 or 2 min PMI displayed good preservation of cell and tissue structure (Figure 1A−C). Therefore, based on the histology, one might expect the greatest biochemical alterations to be observed in cerebellum tissue prepared after a 30 min PMI, relative to <0.5 or 2 min PMI. However, as chemical alterations are the driving mechanism behind alterations to cell and tissue structure, chemical alterations may be present in tissues prepared after the 2 min PMI relative to <0.5 min PMI, which precede the morphological alterations observed in tissues prepared by after a 30 min PMI. This is particularly true for biochemical alterations arising from altered cerebral metabolism and oxidative stress that rapidly occur following the onset of ischemia within the brain. The aim of this study was to determine to what extent postmortem biochemical alterations, detectable by in situ spectroscopic methods such as FTIR and XAS, could be reduced with rapid cryo-preservation of brain tissue.

Biochemical Assays. Triplicate frozen sections of tissue (approximately 100 μm thickness) were collected for biochemical assay of the average lactate and thiol to disulfide ratio in the cerebellum (Table 1). The average concentration of lactate was significantly greater and the thiol to disulfide ratio was significantly decreased at the 2 and 30 min PMIs compared with the <0.5 min PMI ($p < 0.05$). However, there was no significant difference in lactate levels between 2 and 30 min PMI, whereas there was a significant increase in the thiol to disulfide ratio at 30 min relative to 2 min PMI.

Table 1. Biochemical Assay of Lactate and the Ratio of Thiols to Disulfides from Cerebellar Homogenates[a]

method	lactate (mM)	thiol/disulfide ratio
A	6 ± 2	3.3 ± 0.3
B	13 ± 2[b]	2.9 ± 0.1[b]
C	11 ± 2[b]	2.2 ± 0.1[bc]

[a]Data shown as mean ± SD ($n = 4$). A significant difference was tested using a two tailed unpaired Student's t test with a 95% confidence limit ($p < 0.05$). [b]Denotes significant difference of tissue prepared by method B or C, relative to method A. [c]Denotes significant difference of tissue prepared by method C relative to method B.

As demonstrated in Table 1, a significant increase in the bulk lactate concentration of the cerebellum is observed in brain tissue after a 2 or 30 min PMI relative to the <0.5 min PMI, but no significant difference was observed between the 2 and 30 min PMI, which is in strong agreement with the results published by others for these sample preparation methods.[41] Likewise, Table 1 demonstrates that the thiol/disulfide ratio decreased as a function of increased PMI time, consistent with the published literature.[33,34,37−40] It is well established from bulk biochemical assay of whole brain homogenates that lactate levels increase rapidly during the postmortem time interval, reaching a maximum within 2−3 min of ischemia.[35,36,41,42] In addition, the thiol group on the cysteine moiety of glutathione (GSH) is readily oxidized to a disulfide (GSSG), or a mixed protein glutathione disulfide adduct (Pr−S−S−G), and is a key marker of oxidative stress. Therefore, for quantification of cerebral metabolites and markers of oxidative stress, a rapid method of cryo-preservation of brain tissue is required to determine metabolic markers and levels of reduced and oxidized glutathione, and Pr−S−S−G adducts that are preserved at or near to in vivo levels.[33,34,37−40] However, one difference in the determination of thiol redox relative to cerebral metabolites, is that tissue oxidation in air following animal death may be a greater cause of artificial results than ischemic conditions initiated by animal death.[33,34,37−40] Regardless of the exact origin of artificial alterations in sulfur redox following animal death, if a suitable protocol is not employed, the GSSG/GSH ratio increases rapidly following animal death, and differences present in vivo may be lost; this has been the source of many confounding results in previous studies.[33,34,37−40]

To identify whether altered metabolic status or oxidative stress exists within the brain in vivo, rapid cryo-preservation of the brain tissue is required, or the differences may be lost. The three most common methods to rapidly preserve brain tissue for biochemical analyses are whole body immersion in liquid nitrogen, decapitation into liquid nitrogen, and freeze-blowing, with the latter being the most rapid method yielding metabolite levels closest to those in the in vivo state.[35,36,41,42] However, freeze-blowing is destructive, does not retain tissue morphology, and is not suitable for imaging techniques.[35,36,41,42] While removal of the skull from live rats and in situ freezing of the brain in the live animal, or whole body immersion of a live animal into liquid nitrogen is established to better preserve brain biochemical status,[35,36,41,42] these methods do not conform with standard procedures for euthanasia by animal ethics boards. Therefore, decapitation into liquid nitrogen has been employed in this study.

The aim of this investigation was not to determine the optimum sample preparation procedure to preserve brain biochemistry, or to discredit previous work, but rather to demonstrate the nature of biochemical alterations detectable by FTIR and XAS that occur during varying postmortem time intervals.

FTIR Spectroscopic Imaging of Biochemical Markers of Anaerobic Metabolism and Peroxidative Stress. *Discrimination Between Tissue Layers of the Cerebellum Through FTIR Spectroscopic Imaging.* The relative lipid-ester distribution in the cerebellum was determined from the FTIR image generated from second-derivative intensity at 1742 cm^{-1}, assigned to the ester ν(C═O) band (Figure 1G−I). Identification of the three main tissue structures of the cerebellum (white matter, granular layer, molecular layer) was determined via visual comparison of the H&E stained tissue section (Figure 1A−C) with the relative lipid-ester distribution (Figure 1G−I). In addition, hierarchical cluster analysis was applied across the spectral region 1490−1000 cm^{-1} in vector-normalized second-derivative spectra which separated spectra into three clusters, correlated to the molecular, granular, and inner white matter layers (Figure 1D−F), similar to previous reports.[21−23,27,30,43] The average spectrum calculated from each cluster (Figure 2A) was used for the analyses of average biochemical composition of each tissue layer.

Lactate Levels in the Cerebellum. The relative lactate distribution and the change in relative lactate levels were evaluated through second-derivative FTIR spectral intensity at 1127 cm^{-1} as previously described.[21] The FTIR images generated from the second-derivative intensity at 1127 cm^{-1} assigned to the lactate ν(C−O) stretch, for methods A, B, and C, are presented in Figure 1J−L. Visual comparison of the images suggests an increase in relative lactate levels in all three

dx.doi.org/10.1021/cn500157j | ACS Chem. Neurosci. 2015, 6, 226−238

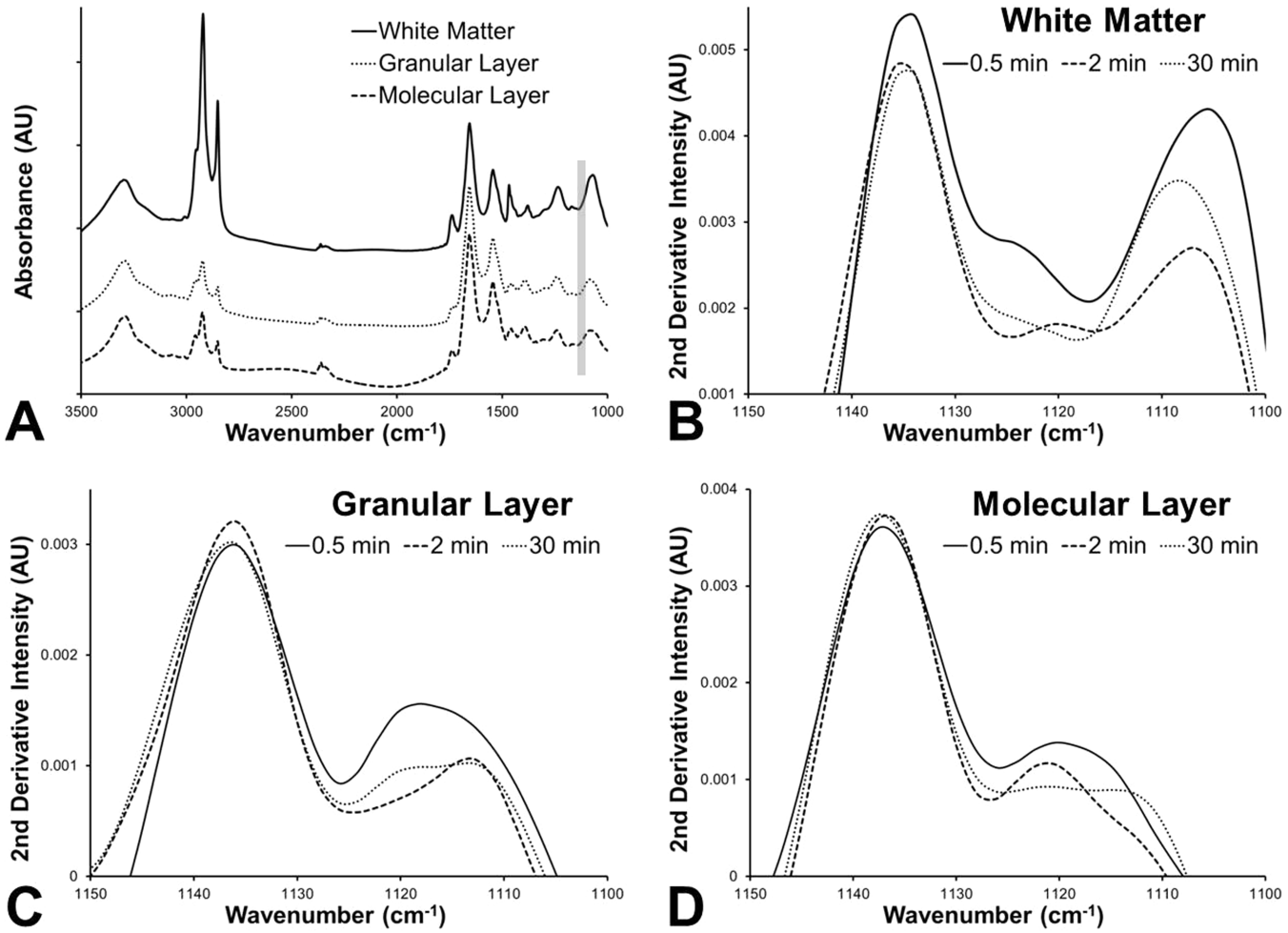

Figure 2. Effect of time period after animal death on FTIR spectra collected from cerebellum tissue layers. (A) Average spectra of tissue layers at the 0.5 min PMI. The lactate region is highlighted by gray shading. Representative examples of second-derivative spectra showing relative lactate levels (1127 cm^{-1}) in (B) white matter, (C) granular layer (gray matter), and (D) molecular layer after 0.5, 2, and 30 min PMI. Note: In second-derivative spectra, increased lactate concentration results in more negative spectral intensity.

Table 2. Second-Derivative FTIR Spectral Intensity Analysis of Relative Levels of Lactate (1127 cm^{-1}) in White Matter (WM), Granular Layer (GL), and Molecular Layer (ML) of the Cerebellum[a]

method	WM 1127	GL 1127	ML 1127
A	$(2.4 \pm 0.4) \times 10^{-3}$	$(10 \pm 1) \times 10^{-4}$	$(1.1 \pm 0.1) \times 10^{-3}$
B	$(1.7 \pm 0.5) \times 10^{-3b}$	$(7 \pm 1) \times 10^{-4b}$	$(9.2 \pm 0.4) \times 10^{-4b}$
C	$(2.0 \pm 0.1) \times 10^{-3b}$	$(6.3 \pm 0.6) \times 10^{-4b}$	$(8 \pm 1) \times 10^{-4b}$

[a]Data shown as mean ± SD (n = 4). Note: In second-derivative spectra, increased relative concentration correlates to lower second-derivative intensity values (i.e., increased intensity in the negative direction). A significant difference was tested using a two tailed unpaired Student's t test with a 95% confidence limit ($p < 0.05$). [b]Denotes significant difference of tissue prepared by method B or C, relative to method A. [c]Denotes significant difference of tissue prepared by method C relative to method B.

structures of the cerebellum (white matter, granular layer, molecular layer) at the 2 and 30 min PMIs, relative to <0.5 min PMI. This was confirmed by analysis of the second-derivative intensity at 1127 cm^{-1} for the average spectra of each tissue layer, which revealed a significant increase in second-derivative intensity at 1127 cm^{-1} at the 2 and 30 min PMIs relative to <0.5 min (Table 2). Thus, FTIR confirmed the results of the biochemical analysis of lactate (Table 1). Representative examples of second-derivative spectra showing this relative increase in lactate content are presented in Figure 2B–D. At all time points, the highest relative lactate content was observed to occur at the boundary of the granular and molecular layers, consistent with the location of the Purkinje neurons. Our previously published analysis of this region at higher resolution with FTIR imaging showed that the highest lactate was found in Purkinje neuron soma,[21] and will not be discussed further in this Article.

Although the same pattern of relative lactate distribution (inner white matter < granular layer ∼ molecular layer) was observed for all samples, there was a net increase in the relative lactate content for each tissue layer in samples prepared after a 2 or 30 min PMI, relative to a PMI of <0.5 min, but no difference was observed between the 2 or 30 min PMI. These results are in direct accordance with those observed from

dx.doi.org/10.1021/cn500157j | ACS Chem. Neurosci. 2015, 6, 226–238

biochemical assay of bulk lactate content in this investigation (Table 1), and the results reported by others.[41] Therefore, the combination of these tissue layer specific results and the results from bulk biochemical assay highlights that in order to successfully image regions with altered metabolic status closest to the in vivo state, rapid cryo-preservation (within 30 s of animal death) is essential.

Abundance of Crystalline Creatine Microdeposits. FTIR spectroscopic images from absorbance at 1402 cm^{-1} (7.1 μm) have been used previously to visualize the location of crystalline creatine microdeposits in brain tissue.[22,24,29,44,45] In this study visible light microscopy was used to locate creatine deposits, and the presence of creatine was confirmed by coarse resolution FTIR imaging with a globar source and focal plane array (FPA). To investigate the chemical composition of the creatine deposits in greater detail, higher spatial resolution wide-field synchrotron radiation Fourier transform infrared focal plane array (SR-FTIR-FPA) imaging was employed. To enable visualization of the creatine deposits at higher spatial resolution, absorbance of the ν(N−H) stretch at 3300 cm^{-1} (3 μm) was used (Figure 3A, B). No chemical differences were observed between the crystalline creatine microdeposits at the different PMIs (Figure 3C); however, there was a significant increase in the number of deposits observed at the 2 and 30 min PMIs relative to <0.5 min in the molecular and granular layers, but not the white matter (Table 3), indicating that crystallization of creatine is an early postmortem event in gray matter. There was no significant difference in the abundance of the deposits between the 2 and 30 min PMIs for any tissue layer (Table 3).

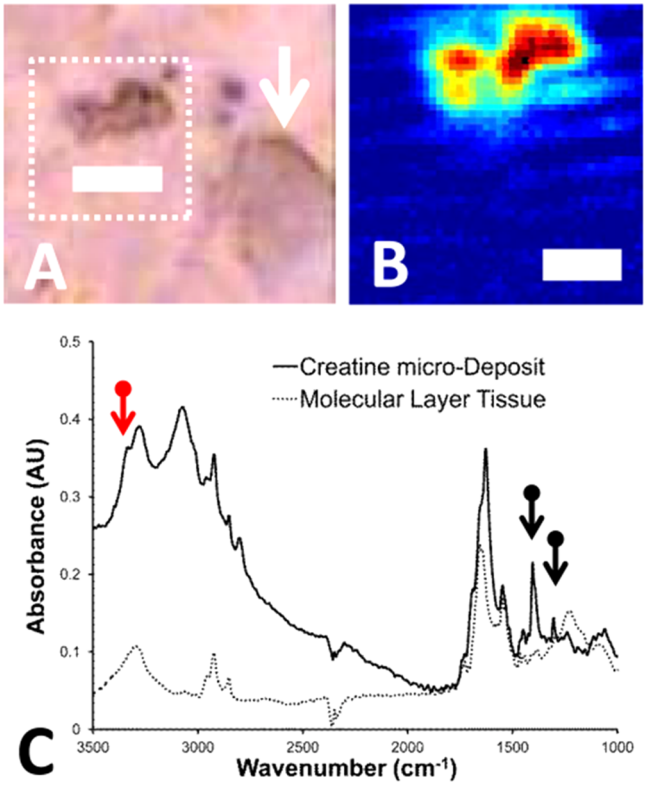

Figure 3. Wide-field SR-FTIR-FPA imaging of creatine microdeposits in cerebellum tissue. (A) Bright field image of unstained tissue highlighting region of analysis around creatine-microdeposit (white dotted box) and an adjacent neuron (white arrow). (B) FTIR image of creatine microdeposit generated from integrated area of the ν(N−H) band at 3300 cm^{-1}. (C) Representative FTIR spectra from creatine deposit and surrounding molecular layer tissue. Red arrow indicates the position of the band at 3300 cm^{-1} used to generate the image from second-derivative spectra shown in B, while black arrows indicate the position of other characteristic creatine bands at 1402 and 1311 cm^{-1}, used in previous studies. Scale bars = 5 μm.

Table 3. FTIR Analysis of the Mean Abundance of Crystalline Creatine Microdeposits per Cerebellum Tissue Section[a]

method	WM	GL	ML
A	ND	0.5 ± 0.5	0.8 ± 0.9
B	ND	3 ± 2[b]	3 ± 1[b]
C	ND	2 ± 1[b]	2.3 ± 0.9[b]

[a]Data shown as mean ± SD (n = 4). A significant difference was tested using a two tailed unpaired Student's t test with a 95% confidence limit (p < 0.05). [b]Denotes significant difference of tissue prepared by method B or C, relative to method A.

It is well established that depletion of high energy phosphates, specifically dephosphorylation of phosphocreatine, is one of the earliest indicators of oxygen and energy deprivation.[36,42] Therefore, an increased creatine to phosphocreatine ratio would be expected in brain tissue collected after a 2 or 30 min PMI, relative to a PMI of <0.5 min. Due to the complex and overlapping nature of absorbance bands in FTIR spectra collected from brain tissue, a direct measurement of the creatine to phosphocreatine ratio cannot be made. However, increased abundance of crystalline creatine microdeposits have been observed in the brain in several neurodegenerative conditions (amylotrophic lateral sclerosis, Alzheimer's disease, epilepsy, and cerebral malaria).[22,24,29,44,45] Further, it was recently established in the case of malarial diseased mice that the deposits do not occur in vivo, but rather are an ex vivo artifact of tissue dehydration.[22] As phosphocreatine is used as an immediate high energy supply and converted to creatine under conditions of oxygen and energy deprivation, regions of high localized creatine concentration must exist. As creatine is less soluble than phosphocreatine, the creatine crystallizes out of solution during dehydration of the tissue sections.[22] As such, crystalline creatine microdeposits can serve as a valuable ex vivo marker of the location of altered energy metabolism that was present in vivo.[22] As would be expected, a greater number of creatine deposits were observed in the cerebellum tissue prepared after a 2 or 30 min PMI, relative to a PMI of <0.5 min, (Table 3, Figure 3), and no significant difference was observed in the number of deposits between 2 and 30 min PMI. Again, these results highlight the importance of rapid cryo-preservation of brain tissue to successfully image the relative concentration and distribution of energy metabolites as close as possible to the in vivo state.

Aggregated Protein Levels in the White Matter, Granular, and Molecular Layers of the Cerebellum. FTIR functional group images of the relative levels of aggregated proteins were generated from the second-derivative intensity at 1625 cm^{-1} (amide I band), as used in other studies.[23,26,27] The false-color images are presented in Figure 1M−O. Visual inspection of the images and analysis of the second-derivative intensity of the average spectra from each tissue layer revealed no significant difference in the relative levels of aggregated proteins between the three PMIs for any tissue layer (Table 4).

Based on the significant tissue damage and edema observed in the cerebellum prepared after a 30 min PMI relative to a PMI

dx.doi.org/10.1021/cn500157j | ACS Chem. Neurosci. 2015, 6, 226−238

Table 4. Second-Derivative FTIR Spectral Intensity Analysis of Relative Levels Aggregated Proteins (1625 cm^{-1}) in White Matter (WM), Granular Layer (GL), and Molecular Layer (ML) of the Cerebellum[a]

method	WM 1625	GM 1625	ML 1625
A	$(9 \pm 1) \times 10^{-3}$	$(1.0 \pm 0.1) \times 10^{-2}$	$(1.2 \pm 0.1) \times 10^{-2}$
B	$(7.6 \pm 0.8) \times 10^{-3}$	$(0.9 \pm 0.6) \times 10^{-2}$	$(1.2 \pm 0.1) \times 10^{-2}$
C	$(8.4 \pm 0.5) \times 10^{-3}$	$(1.0 \pm 0.1) \times 10^{-2}$	$(1.9 \pm 0.1) \times 10^{-2}$

[a]Data shown as mean ± SD (n = 4). Note: In second-derivative spectra, increased relative concentration correlates to more negative second-derivative intensity. A significant difference was tested using a two tailed unpaired Student's t test with a 95% confidence limit ($p < 0.05$). [b]Denotes significant difference of tissue prepared by method B or C, relative to method A. [c]Denotes significant difference of tissue prepared by method C relative to method B.

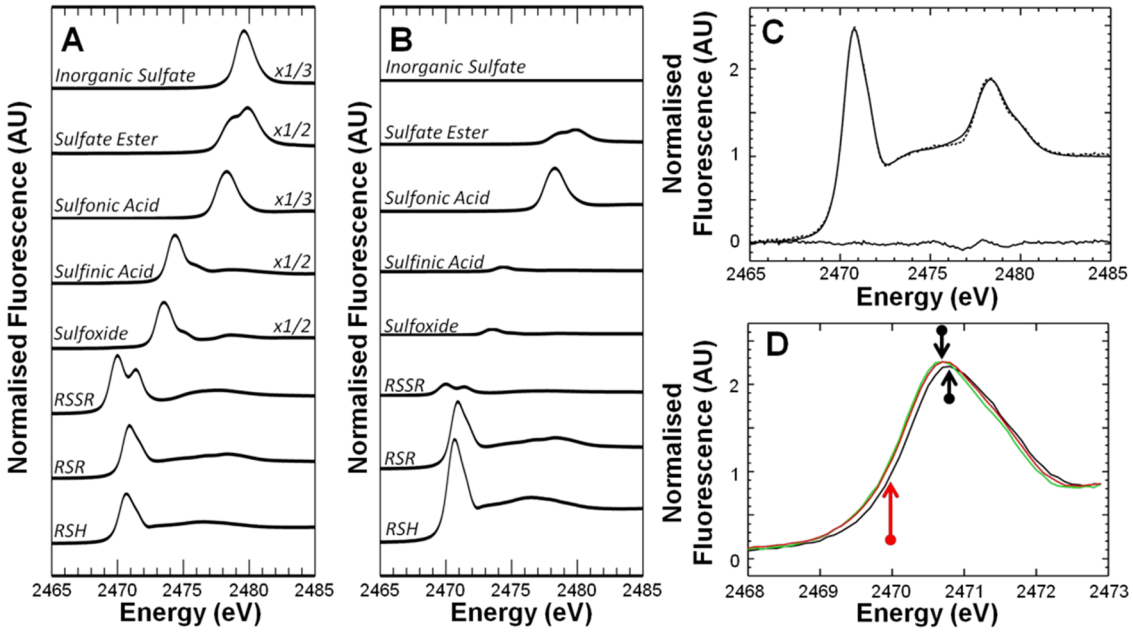

Figure 4. Sulfur K-edge XAS analysis of the effect of time period after death on sulfur speciation within the cerebellum. (A) Sulfur K-edge spectra of model compounds of different chemical forms of sulfur. RSH, thiol; RSR, thioether; RSSR, disulfide. (B) Sulfur K-edge spectra of model compounds scaled to the relative contribution to the fit presented in (C). (C) Representative example of sulfur K-edge XAS fit for cerebellum tissue. (D) Alterations to the sulfur K-edge due to variation in thiol, thioether, and disulfide contribution. Black < 0.5 min, green = 2 min, red = 30 min post death. Red arrow indicates increased absorbance at ~2469.8 eV due to increased contribution of disulfides. Black arrows indicate shift of maximum absorbance to lower energy due to increased contribution of disulfides, and decreased contribution of thiols and/or thioethers.

Table 5. XAS Sulfur Fitting Results of the Relative Contribution (%) of Different Chemical Forms of Sulfur to the Total Sulfur Pool in Cerebellum with Varying Postmortem Interval[a]

method	RSH	RSR	RSSR	sulfoxide	sulfinic acid	sulfonic acid	sulfate ester
A	43 (1) ± 7	32 (1) ± 2	6 (0.4) ± 1	1.7 (0.2) ± 0.4	1.2 (0.2) ± 0.1	7.7 (0.1) ± 0.4	9 (0.2) ± 5
B	54 (2) ± 10	16 (2) ± 7^b	10 (0.6) ± 3^b	2.1 (0.3) ± 0.5	1.3 (0.3) ± 0.3	9 (0.2) ± 2	8 (0.3) ± 4
C	46 (2) ± 9	21 (1) ± 5^b	9 (0.6) ± 2^b	1.5 (0.3) ± 0.2	0.8 (0.3) ± 0.1^{bc}	6 (1) ± 2	16 (0.2) ± 6

[a]Values given are the average percentages ± standard deviation of replicate measurements from 4 animals. The values in parentheses are the average estimated standard deviation from the individual fits (given as the last digit of the percentage) obtained from the diagonal elements of the covariance matrices. The estimated standard deviation gives an indication of the precision of determination of the value in the least-squares fit whereas the standard deviation of replicate measurements gives an indication of how much variation is present between different samples. As expected for slightly different individual fits, the average percentages do not total to 100%, although the individual fits do total to 100%. A significant difference was tested using a two tailed unpaired Student's t test with a 95% confidence limit ($p < 0.05$). [b]Denotes significant difference of tissue prepared by method B or C, relative to method A. [c]Denotes significant difference of tissue prepared by method C relative to method B.

of <0.5 or 2 min, one might expect a substantial increase in the levels of aggregated proteins. However, an important difference between ischemic conditions created in the brain by animal death in this investigation, and true ischemic conditions during global brain ischemia, is the lack of reperfusion following animal death. Therefore, although the brain tissue will suffer energy deprivation, increased free radical generation, and antioxidant depletion following animal death, the huge spike in free radical production that occurs following the return of oxygen (reperfusion) to ischemic tissue is not present in decapitation-inflicted brain ischemia.[33,34,37−39] Hence, levels of tissue oxidation products (i.e., protein aggregates) following decapitation may be substantially lower than those in a clinically relevant model of global brain ischemia with reperfusion. Indeed, in this investigation, no significant differences in the level of aggregated proteins (second-derivative intensity at 1625

dx.doi.org/10.1021/cn500157j | ACS Chem. Neurosci. 2015, 6, 226−238

cm^{-1}, which is an established marker of protein oxidation) were observed in any cerebellum tissue layer as a result of postmortem interval. This result is important, as it demonstrates that although rapid cryo-preservation is required to study metabolic and thiol redox status of the brain (discussed next), investigation of the protein secondary structures and protein oxidation may be performed on flash-frozen brain tissue which is dissected first before flash-freezing, rather than after decapitation into liquid nitrogen. The latter adds a significant time investment to chisel out the frozen brain from the head.

XAS Analysis of the Effect of Time Post Death on the Average Speciation of Sulfur in the Cerebellum. The average thiol, thioether, disulfide, sulfoxide, sulfinic acid, sulfonic acid, and sulfate ester proportions for the cerebellum at <0.5, 2, and 30 min PMI were determined in situ from bulk XAS spectra collected at the sulfur K-edge, as previously described.[1] An example of the fitting process is presented in Figure 4A−C, and representative spectra of the cerebellum collected at each time point presented in Figure 4D. Levels of sulfur species are expressed as the percentage of the total sulfur detected (Table 5), and thus, the value for disulfide (RSSR) is the percentage of sulfur atoms present as disulfide. Relative disulfide levels were found to increase significantly, and relative thioether levels found to decrease significantly, at time points 2 and 30 min PMI relative to <0.5 min (Table 5). There was no significant difference in disulfides or thioethers between the 2 and 30 min PMIs (Table 5). In addition, there was a significant decrease in the sulfinic acid content at 30 min relative to <0.5 and 2 min post animal death (Table 5).

Due to the rapid oxidation of tissue thiols to disulfides in air,[33,34,37−40] a method of in situ detection that does not require tissue dissection, homogenization, or extraction would be preferable. Although this was not previously available to the neuroscience field, XAS at the sulfur K-edge may be one such technique with these capabilities. The method has been demonstrated as a novel approach to study thiol redox in situ within biological samples,[1,46−48] and recently validated to study thiol redox and sulfur speciation in brain tissue.[1] Further, the use of a helium cryostream is compatible with XAS measurements at the sulfur K-edge and has the advantage of minimizing thiol oxidation due to air-exposure,[1] minimizing spectral distortion due to X-ray absorption by argon, and also minimizing photo-oxidation of sulfur (see Supporting Information Figure 1).[49] Consequently, in situ determination of thiol and disulfide levels in flash frozen tissue sections under cryogenic conditions using XAS at the sulfur K-edge has considerable advantages for determining thiol redox as close as possible to the in vivo state. It should be noted that the spectral alterations presented in Figure 4 are relatively subtle. However, as can be seen in Supporting Information Figure 1, two replicate spectra of the same sample are essentially superimposed. Likewise, Supporting Information Figure 1 demonstrates that beam damage is not visually observable between two replicate sweeps under inert (helium or vacuum) conditions. Therefore, although the spectral alterations presented in Figure 4 are subtle, they are not the result of beam damage or experimental error, but reflect the subtle biochemical alterations as a consequence of the PMI, which are statistically significant as demonstrated from 4 biological (animal) replicates (Table 5). The individual spectra from the 4 biological replicates for method A and for method B are plotted in Supporting Information Figure 2, which highlights the reproducibility of the observed alterations.

There are several important considerations for the use of XAS at the sulfur K-edge to study thiol redox, especially when compared with the established literature on sulfur redox derived from traditional biochemical assays. Tissue microdissection, homogenization, and extraction prior to biochemical assay can lead to artificial thiol oxidation, which is one disadvantage of biochemical assays compared to direct in situ analysis using XAS. However, the homogenization and extraction process, along with the method of detection often add chemical specificity to biochemical assays which can not be obtained from XAS. For example, biochemical assays routinely quantify reduced and oxidized glutathione, or quantification of protein thiols and protein disulfides.[34] In contrast, although it is common practice to fit XAS spectra to reduced and oxidized glutathione model compounds, only the total thiol and total disulfide levels can be quantified.[1,46−48] Further, it is essential to take into account the contribution of nonthiol organic sulfides, thioethers, in XAS measurements. In several studies, only a total sulfide value (thiols + thioethers) was reported. Therefore, conclusions drawn regarding oxidative stress from a total sulfide/disulfide ratio from XAS data, may be inaccurate if the contribution of thioether is neglected.

In this study, a significant increase in the level, relative to total sulfur, of total disulfides, and a significant decrease in thioether, but not thiols, were observed from XAS measurements of cerebellum tissue prepared after 2 or 30 min PMI, relative to *a* < 0.5 min PMI (Table 5). The increase in disulfides is in strong agreement with the postmortem oxidation of reduced glutathione to oxidized glutathione or Pr−S−S−G adducts as previously reported.[34] The decrease in thioethers most likely results from consumption of *S*-adenosyl-methionine (SAM) and a shift in equilibrium of methionine metabolism toward homocysteine production to allow continued methylation and adenosine production under ischemic conditions.[50−53] As no increase in sulfoxides was observed, loss of methionine due to oxidation to methionine sulfoxide is unlikely. As biochemical assays demonstrate deceased reduced glutathione and increased oxidized glutathione during ischemia and/or the PMI, decreased thiols might have been expected to occur concomitant with increased disulfides measured by XAS. However, as XAS determines total thiols, a shift in methionine metabolism back to homocysteine production during the PMI would result in an increase in total thiols, which may negate the loss of thiols due to oxidation to disulfides. These results highlight several important considerations for interpretation of XAS spectra at the sulfur K-edge. First, rapid cryo-preservation of brain tissue is essential to prevent artificial oxidation and formation of disulfides due either to ischemic conditions created at the time of animal death, or to air-exposure during tissue dissection. Second, although a simple measurement of sulfides and disulfides can be made from XAS spectra, which will likely be in good agreement with mechanisms of oxidative stress following brain ischemia, this approach is too simplistic. In fact, the total sulfide and disulfide levels are influenced by not only thiol oxidation, but also methionine homeostasis, methionine oxidation, and protein synthesis. Therefore, for a more accurate "picture" of thiol redox status, XAS spectra at the sulfur K-edge should be fitted to determine thiol, disulfide, thioether, and sulfoxide contributions.

This investigation is the first report of rapid loss of thioether due to onset of ischemic conditions within the brain, although alterations in the methionine metabolic pathway have been previously reported.[55] As the decrease in thioether in this study

did not correspond to an increase in sulfoxides, loss of thioether is likely not the result of oxidation of thioether to sulfoxides. More likely, the loss of thioether arises from a shift in methionine metabolic homeostasis, or enzymatic degradation.[55] As decapitation is a simple and one of the earliest animal models of brain ischemia without reperfusion, this result is of direct relevance to future studies of biochemical alterations induced in a more clinically relevant model of global brain ischemia with reperfusion, such as the two-vessel occlusion model. As *S*-adenosyl-methionine is crucial for methylation reactions and protein synthesis,[55] and decreased protein synthesis is observed after global ischemia,[56] this could account for the neuroprotective properties of SAM administration in animal models of brain ischemia.[57] Therefore, the ability to directly monitor (and potentially image) thioether levels in situ will be of great benefit in future studies aimed at understanding the exact biochemical mechanisms of delayed neurodegeneration several days after ischemic insult.[58] This could be of great importance for the development of improved patient therapy.

Both the XAS and biochemical assay results of this investigation highlighted alterations in sulfur speciation, with increased disulfides (XAS) or increased disulfide to thiol ratio (biochemical assay) as a consequence of a 2 min PMI (relative to <30 s). However, the XAS detected no significant difference in disulfide levels between the 2 and 30 min PMI, whereas the biochemical assay identified an increase in disulfide to thiol ratio during this period. A possible explanation for this result is a greater fraction of non-GSSG disulfides in the supernatant fraction of brain homogenates assayed from tissue prepared with a PMI of 30 min. Significant edema was evident on histological examination at this time point, and therefore autolytic processes were likely to have begun, including proteolysis. The latter could result in a large increase of peptide disulfides in the supernatant fraction of brain homogenates. Therefore, the fact that the biochemical assay detection is not specific to GSH or GSSG, but rather detects total thiols and disulfides in the supernatant fraction of tissue homogenates (for which GSH and GSSG are normally the major components) should be kept in mind when interpreting these results. In addition, the XAS analysis was performed with a 2×4 mm^2 beam, centered on a tissue section approximately 5×5 mm^2 in size. Therefore, the outside edges of the tissue were not analyzed by XAS, whereas these tissue components were analyzed by biochemical assay. As it is well established that air-oxidation at the sample surfaceis a major contributor to an increased disulfide to thiol ratio,[1,39] this could also explain the differences observed between the XAS and biochemical assay results, as the surface of the sample was not anlayzed in the XAS measurement (i.e., the beam was positioned within the sample and did not encompass the sample edge).

As it is known that taurine is rapidly released from brain cells under ischemic conditions, differences in the sulfonic acid levels at the cellular or subcellular level would be expected between the different tissue preparation methods used in this study. As taurine is chemically and metabolically stable (relative to thiols), alterations in sulfonic acid levels would be expected to result from redistribution rather than chemical alteration. Therefore, as an imaging modality was not employed in this study, alterations in cellular distribution could not be investigated, and it is not surprising that no significant differences in the bulk levels of sulfonic acid were detected. However, hypotaurine, a reactive intermediate in the pathway to taurine synthesis, is likely to be the major contributor to the sulfinic acid signal detected by XAS at the sulfur K-edge.[1] As a metabolic/catabolic and redox active intermediate,[59] hypotaurine levels are not likely to remain stable in brain tissue, which would account for the decreased sulfinic acid signal observed in cerebellum tissue prepared by the longest, 30 min PMI, relative to 2 and <0.5 min PMI. However, it must be noted that the small sulfinic acid signal detected in this study is likely only present in concentrations that are just sufficient for detection. Small variations in noise may have a large effect on the determined concentration. Supporting Information Figure 3 shows a representative example where two minor chemical components (sulfoxide and sulfinic acid) are included in the fit, and then the fitting process repeated without each of the individual components. Removal of sulfoxide results in the residuals increasing by a factor of 2, however, removal of the sulfinic acid component results in only a very subtle increase in the residual. Indeed, the fitting process without the inclusion of sulfinic acid visually appears "reasonable". Therefore, interpretation of the results for sulfinic acid must be viewed with care due to its small and variable contribution to the total sulfur pool.

Future Work. Liquid nitrogen, though readily available and commonly used for rapid freezing of samples in many laboratories, may not be the ideal cryogenic freezing agent. This is because the well-known Leidenfrost effect, arising from a skin of gaseous (nitrogen) vapor that provides thermal insulation will substantially increase the time to freeze the sample. The Leidenfrost point signifies the onset temperature of formation of the stable gaseous film, and while this is difficult to estimate without measurement it will be at least 100 °C above the boiling point of a liquid gas. Thus, for a sample at 37 °C, a cold liquid gas below its Leidenfrost point, such as liquid isobutane (freezing point, −160 °C; boiling point, −12 °C) may provide faster freezing than liquid nitrogen. Alternatively, the use of a cold liquid that will not form a gaseous film such as isopentane (freezing point, −160 °C; boiling point, 28 °C) provides another option, although unfortunately isopentane tends to become very viscous at temperatures approaching its freezing point and thus may not be ideal. Rates of cooling are obviously complex, and future work will investigate different cryogens to provide more optimal freezing conditions.

■ CONCLUSION

This study is the first to demonstrate that the same experimental considerations for bulk biochemical analyses of metabolic and antioxidant species are also required for in situ spectroscopic studies, an often overlooked fact. For determination of markers of altered brain metabolism such as lactate or crystalline creatine microdeposits that accurately reflect the in vivo state and for determination of thiol redox as close as possible to the in vivo state, rapid cryo-preservation (i.e., decapitation into liquid nitrogen) and analyses of frozen hydrated sections under cryogenic conditions is essential. Many previous biospectroscopic studies have used flash-frozen tissue that was frozen after the brain was first dissected from the head, which is in direct contrast to protocols recommended for analysis of metabolites and oxidation products; such methodological oversights could potentially remove differences between a control and disease state that were present in vivo. Despite the alterations observed for metabolites (lactate and creatine) and oxidation markers (thiol/disulfides), other biochemical markers of oxidative stress, such as aggregated protein content, appeared unchanged. The extent that biochemical alterations in

the window between animal death and tissue freezing may confound studies of disease pathogenesis was not studied in this investigation and remains to be determined. As such, this study should not serve to discredit any previous work, but rather highlight that the choice of protocol for obtaining representative brain tissue and the postmortem time interval are critical considerations for future biospectroscopic investigations. If brain tissue is dissected from the animal and then frozen, the biochemical results should not be considered to truly represent the in vivo state. Rather, the tissue represents a mildly ischemic brain, even in the control animal group. This study is the first report of rapid loss of thioether following onset of ischemic conditions in the rat brain, and may have significant relevance to impaired neuron function and delayed neurodegeneration after brain ischemia, which will be investigated further in future studies. To the best of our knowledge, this is the first ever report of FTIR and XAS analysis of brain tissue prepared by rapid cryo-preservation (decapitation into liquid nitrogen). It is expected that this sample preparation protocol will be of great benefit for future in situ investigation of the role of anaerobic metabolism, antioxidants, and peroxidative stress during brain ischemia and neurodegenerative conditions.

METHODS

Chemicals. Unless stated otherwise, all kits and chemicals were purchased from Sigma-Aldrich.

Animal Handling and Tissue Preparation. Cerebellum was obtained from healthy 6 week old male Sprague−Dawley rats (n = 4). Rats were housed with a 12 h light/12 h dark cycle with ad libitum access to chow and water. This work was approved by the University of Saskatchewan's Animal Research Ethics Board, and adhered to the Canadian Council on Animal Care guidelines for humane animal use. Animals were anesthetized with isoflurane and humanely sacrificed through decapitation. Following decapitation, three sample preparation protocols were followed to yield postmortem intervals of less than 30 s, 2 min, or 30 min. With method A, the head was immediately flash frozen in liquid nitrogen cooled isopentane. We estimate that the time for complete freezing was less than 30 s. The brain was then chiseled out from the frozen rat head at dry ice temperature. With method B, the brain was rapidly dissected from the skull, placed in optimal cutting temperature (OCT) medium, and flash frozen in liquid nitrogen cooled isopentane, which took approximately 2 min. With method C, the brain was dissected from the skull, placed in OCT, and allowed to stand for 30 min before flash-freezing as described for method B. All samples were stored at −80 °C until required for analyses.

Tissue Sectioning for Spectroscopic Analyses and Biochemical Assays. The cerebellum was chosen in this investigation due to its ordered structure, and the fact that it is a well characterized brain region, which makes it ideal for methods-based and proof of principle studies. Further, altered neurochemistry of the cerebellum is implicated in certain neurological diseases and disorders, making the results of this study valuable from both a methods based and a disease mechanism point of view. Triplicate, 10 μm thick sections of the cerebellum from 4 animals from each of the three sample preparation groups were cut on a cryo-microtome at −16 °C and melted onto either glass microscope slides for routine histology, CaF_2 membranes (Crystran Inc.) for FTIR spectroscopic analysis, or Thermanox plastic coverslips for sulfur K-edge XAS analysis. Tissue sections were air-dried and immediately analyzed (within 2 h) for FTIR spectroscopic analyses, or maintained at dry ice temperature (or below) for a period of 2−5 days prior to sulfur K-edge XAS analysis. Due to the known effect of storage conditions on infrared spectra collected from biological samples,[60] sections were stored in a desiccator, in the dark, and at room temperature prior to analyses. In addition to tissue sections for spectroscopic analyses, an additional six 100-μm-thick sections were cut from each brain for biochemical assay. Three sections from each set of 6 were used for assay of brain lactate, and three sections were used for assay of the GSSG/GSH ratio.

Lactate Assay. The supernatant fraction of brain homogenates was prepared from three pooled 100 μm thick tissue sections. The tissue sections were reduced to a fine powder via pulverization under liquid nitrogen, and the powder dissolved in phosphate buffered solution. The supernatant was separated from the pellet via centrifugation at 10 000g and deproteinized with a 10 kDa MWCO spin filter to remove endogenous lactate dehydrogenase. The lactate concentration of the supernatant was determined using an enzymatic lactate assay kit (MaAK065 Sigma-Aldrich) according to the manufacturer's instructions.

GSH and GSSG Assay. The supernatant fraction of brain homogenates was prepared from three pooled 100 μm thick tissue sections. The tissue sections were reduced to a fine powder via pulverization under liquid nitrogen, and the powder dissolved in phosphate buffered solution. The supernatant was separated from the pellet via centrifugation at 10 000g. The thiol component of the supernatant fraction, for which reduced glutathione is the dominant source, was quantified by absorbance at 412 nm following reaction with 5,5-dithiobisnitrobenzoic acid (Sigma-Aldrich). The disulfide component of the supernatant fraction, for which oxidized glutathione is the dominant source, was quantified by absorbance at 340 nm following incubation with glutathione reductase and NADPH.

FTIR Spectroscopic Analyses. Globar-FTIR-FPA spectroscopic images were collected at the Canadian Light Source (CLS) with a Hyperion 3000 microscope fitted with an upper objective of 15× magnification and a numerical aperture of 0.6, combined with a lower condenser of 15× magnification and 0.4 numerical aperture. This arrangement yielded a pixel size of 2.65 μm, which was later subjected to 2 × 2 pixel binning to yield an effective image pixel size of 5.3 μm. Globar-FTIR-spectroscopic images were collected with a spectral resolution of 4 cm^{-1} and the coaddition of 128 scans, with a background image similarly collected from blank substrate using 128 coadded scans. The background was collected immediately prior to each sample. We note that FTIR spectroscopic analyses were performed under ambient laboratory conditions, and not cryogenic conditions as for XAS analyses. Please refer to Supporting Information Figure 4 for a discussion of this topic.

SR-FTIR-FPA spectroscopic images of microcreatine deposits were collected at both the Canadian Light Source and at the Synchrotron Radiation Center (SRC) in Wisconsin. At the CLS, images were collected with a Hyperion 3000 microscope fitted with an upper objective of 52× magnification and a numerical aperture of 0.6, combined with a lower condenser of 15× magnification and 0.4 numerical aperture. This arrangement yielded a pixel size of 0.77 μm. The incident infrared beam was focused and aligned to the center of the array, and then defocused such that an array area of approximately 28 μm × 28 μm (36 × 36 pixels) was illuminated by light. During data processing individual images were cropped to a region consisting of 36 × 36 pixels, and 2 × 2 pixel binning performed to yield a final image of 18 × 18 pixels (1.54 μm effective pixel size), with adequate spectral signal-to-noise within each pixel. SR-FTIR-spectroscopic images were collected with a spectral resolution of 4 cm^{-1} and the coaddition of 1024 scans, with a background image collected from blank substrate using 1024 coadded scans. The background was collected immediately prior to each sample. Normalization to beam current was not performed. At the SRC, images were collected similar to methods previously described.[61] In general, images were collected from a Hyperion 3000 microscope fitted with an upper objective of 74× magnification and a numerical aperture of 0.65, and a lower condenser of 15× magnification and 0.6 numerical aperture. This arrangement yielded an effective pixel size of 0.54 μm × 0.54 μm. The incident infrared beam was focused and aligned to the center of the array, and then defocused to cover the complete array (34.6 μm × 34.6 μm). SR-FTIR-spectroscopic images were collected with a spectral resolution of 4 cm^{-1} and the coaddition of 512 scans. A background image was collected from blank substrate using 1064 coadded scans. The background was collected immediately prior to each sample. Normalization to beam current was not performed.

FTIR Spectroscopic Data Analysis. All data processing and image generation was performed using Cytospec software (Cytospec, version 1.2.04) and Opus software (version 6.5, Bruker, Ettlingen, Germany). Raw spectra were vector-normalized to the amide I band (1690−1610 cm^{-1}), and second-derivatives calculated with a Savitsky-Golay 9 point smoothing average. False color functional group images of the relative concentration of lipid, β-sheet aggregates, and lactate were generated from second-derivative intensities at 1742,[23] 1625,[27] and 1127 cm^{-1},[21,62] respectively. Due to the strong increase in signal intensity due to the highly ordered structure of crystalline creatine, images of crystalline creatine deposits were generated from integrated band area of raw spectra at 3300 and or 1402 cm^{-1}.[22,24,29,44,45,63] Hierarchical cluster analysis was performed using the fingerprint spectral region 1490−1000 cm^{-1} to assign spectra to three clusters, which correlated strongly with the histological location of the cerebellum molecular layer, granular layer (gray matter), and inner white matter layer. The average spectra from each cluster were then used for statistical analysis to compare biochemical differences within each tissue region among the three different sample preparation methods (A, B, C). A significant difference in the mean FTIR second-derivative spectral intensity from triplicate tissue sections prepared from four animals between each sample preparation method (i.e., a total of 12 tissue sections per method) was determined with a Student's t test and a 95% confidence interval ($p < 0.05$). For each animal, the average spectral intensity was calculated, and then the t test was performed. Specifically, a separate t test was performed to compare the lactate, creatine, or aggregated protein content of brain tissue prepared by method A versus B, A versus C, and B versus C. The p values from the statistical analyses are presented in Supporting Information Tables 1−5. We note that second-derivative analysis of FTIR spectra is often unreliable for analysis of total concentration of chemical species. However, under the assumption of constant bandwidth, this method is widely used for study of relative changes in chemical composition, as described and justified previously.[21,27]

Sulfur K-edge XAS Data Collection. All sulfur K-edge spectra of cerebellum tissue to compare the effects of the time period after animal death were collected at the Stanford Synchrotron Radiation Lightsource, using beamline 4-3, and employing a Si(111) double monochromator. The incident beam was reduced to 2 × 6 mm^2 by vertical and horizontal slits, and intensity was measured with a helium gas filled I_0 ion chamber. Samples (tissue sections and solutions) were mounted at 45° to the incident beam, and X-ray fluorescence collected with a Stern−Heald−Lytle detector filled with nitrogen gas. Prior to spectra collection, the sample chamber was purged with He to remove air and any water vapor that may condense on the tissue surface, until the relative O_2 content within the chamber was less than 0.5%. X-ray absorption spectra were calibrated against the spectrum of a $Na_2S_2O_3.5H_2O$ powder solid standard, with the lowest energy peak set to 2469.2 eV, as described previously.[46−48,64,65] Spectra acquisition was controlled with the XAS-Collect data collection software,[66] with spectra collected across the energy range 2450−2515 eV, with a total collection time of approximately 5 min. Tissue sections were analyzed under cryogenic conditions with a helium cryostream, as previously reported.[1] The temperature of the Thermanox coverslip, as measured with a thermocouple, was approximately −40 °C. Spectra of calibration standards and model compounds were recorded at room temperature. Samples were transferred from an airtight sealed container on dry ice into the cryostream in less than 5 s. Evidence for ice crystal formation on the tissue surface (i.e., X-ray diffraction peaks in spectra) was only observed in tissue sections for which transfer took longer than 30 s. Model compounds used for fitting routines were representative of disulfides (oxidized glutathione), thiols (reduced glutathione), thioethers (methionine), sulfoxides (methionine sulfoxide), sulfinic acids (hypotaurine), sulfonic acids (taurine), sulfate esters (dextran sulfate), and inorganic sulfates (Na_2SO_4) functional groups and were measured as solutions (to minimize the self-absorption artifacts and spectral differences due to crystal packing, as previously reported),[48,64] made up to 30−100 mM in PBS at pH 7.4 (except for dextran sulfate which was analyzed at pH 8.2). Solutions were analyzed in sulfur free polycarbonate cells with a polypropylene window (built in house).

To investigate the effect of radiation damage on the speciation of sulfur within brain tissue, sulfur K-edge XAS data were collected at the Canadian Light Source, using the soft X-ray microcharacterization beamline (SXRMB) and employing a Si(111) double crystal monochromator. The incident beam was reduced to 2 × 4 mm^2 by vertical and horizontal slits, and intensity measured with a helium gas filled I_0 ion chamber. Samples (tissue sections and solutions) were mounted at 45° to the incident beam, and X-ray fluorescence collected with a 4 element Si drift detector. Prior to spectra collection, the sample chamber was purged with He until the relative O_2 content within the chamber was less than 0.5%. Duplicate spectra were recorded. Following spectra collection, the purge was broken and the sample exposed to beam for 1 min under ambient conditions. Following the 1 min "beam + air" exposure, the sample chamber was purged as described above, and duplicate spectra collected again. X-ray absorption spectra were calibrated against the spectrum of a $Na_2S_2O_3 \cdot 5H_2O$ powder solid standard, with the lowest energy peak set to 2469.2 eV, as described previously. Spectra were collected across the energy range 2450−2515 eV, with a total collection time of approximately 10 min. All spectra were recorded at room temperature.

Sulfur K-edge XAS Data Analysis and Processing. Spectra were processed using the EXAFSPAK suite of programs.[67] Using the DATFIT program, spectra collected from tissue sections were fitted with a linear combination of reference spectra (see standard compounds discussed above). Standards were excluded from the refinements algorithm if they contributed to <0.5% of the total spectra, at a value less than three times their standard deviation of measurement (calculated from the diagonal elements of the variance-covariance matrix). A significant difference in the mean composition of the individual sulfur components between sample preparation methods A, B, and C was determined with a Student's t test and a 95% confidence limit ($p < 0.05$). For example, an individual t test was applied to determine if a significant difference was present between the average thiol content of brain tissue prepared by method B versus method A. A separate t test was performed to test for a significant difference in the thiol content of method C versus method A. A separate t test was applied to test for a significant difference in the thiol content between method C and method B. This process was repeated for each of the different chemical forms of sulfur. The average and standard deviation was calculated for each experimental group using four biological replicates (separate animals) within each group (i.e., $n = 4$). The p values from the statistical analyses are presented in Supporting Information Tables 1−5.

Histology. Routine histology was performed for tissue sections mounted on glass microscope slides, as well as all tissue sections mounted on CaF_2 membranes and Thermanox plastic following spectroscopic analyses. Tissue sections were fixed with formaldehyde vapor released from heating dry paraformaldehyde powder at 80 °C for 2 h. The tissue sections were allowed to equilibrate back to room temperature and remained sealed in the presence of formaldehyde vapor for a further 2 h. Tissue sections were then stained with Mayer's hematoxylin and eosin for routine histological analysis.

Statistics. For all experiments, a significant difference was tested for with a two tailed unpaired Student's t test with a 95% confidence limit ($p < 0.05$). For each experiment, three separate t tests were applied to determine if a significant difference was present between the average analyte content of brain tissue prepared by method B versus method A. A separate t test was performed to test for a significant difference in the analyte content of method C versus method A. A separate t test was applied to test for a significant difference in the analyte content between method C and method B.

■ ASSOCIATED CONTENT

Supporting Information

The nature of photo-oxidation of tissue samples during experiments. This material is available free of charge via the Internet at http://pubs.acs.org.

AUTHOR INFORMATION

Author Contributions

M.J.H., P.G.P., H.N., I.J.P. and G.N.G. conceived and designed the experiments and wrote the paper; M.J.H. prepared the samples and analyzed the data; M.J.H., C.J.B., I.J.P. and G.N.G. conducted the experiments.

Funding

This work was supported by a joint Canadian Institutes of Health Research (CIHR)/Heart and Stroke Foundation of Canada team grant; Synchrotron Medical Imaging (SMI) CIF99472, awarded to H.N., P.G.P., I.J.P., G.N.G., and others. During the course of this study, M.J.H. was a Saskatchewan Health Research Foundation postdoctoral fellow, and is currently a Canadian Institute of Health Research (CIHR) postdoctoral fellow, a SMI postdoctoral fellow, and a fellow in the CIHR-Training grant in Health Research Using Synchrotron Techniques (CIHR-THRUST) (I.J.P. and others). G.N.G. and I.J.P. are Canada Research Chairs. C.J.B. was supported by a Saskatchewan Health Research Foundation Phase 2 Research Grant to H.N., I.J.P, G.N.G., and others and by CIHR-THRUST.

Notes

The contents of this publication are solely the responsibility of the authors and do not necessarily represent the official views of NIGMS or NIH.

The authors declare no competing financial interest.

ACKNOWLEDGMENTS

This work is based in part upon research conducted at the Synchrotron Radiation Center that is primarily funded by the University of Wisconsin—Madison with supplemental support from facility Users and the University of Wisconsin—Milwaukee. Research described in this paper was performed at the Canadian Light Source, which is supported by the Natural Sciences and Engineering Research Council of Canada, the National Research Council Canada, the Canadian Institutes of Health Research, the Province of Saskatchewan, Western Economic Diversification Canada, and the University of Saskatchewan. Use of the Stanford Synchrotron Radiation Lightsource, SLAC National Accelerator Laboratory, is supported by the U.S. Department of Energy, Office of Science, Office of Basic Energy Sciences under Contract No. DE-AC02-76SF00515. The SSRL Structural Molecular Biology Program is supported by the DOE Office of Biological and Environmental Research, and by the National Institutes of Health, National Institute of General Medical Sciences (including P41GM103393).

ABBREVIATIONS

XAS, X-ray absorption spectroscopy; FTIR, Fourier transform infrared

REFERENCES

(1) Hackett, M. J., Smith, S. E., Paterson, P. G., Nichol, H., Pickering, I. J., and George, G. N. (2012) X-ray Absorption Spectroscopy at the Sulfur K-Edge: A New Tool to Investigate the Biochemical Mechanisms of Neurodegeneration. *ACS Chem. Neurosci. 3*, 178−185.

(2) Bohic, S., Murphy, K., Paulus, W., Cloetens, P., Salomè, M., Susini, J., and Double, K. (2008) Intracellular chemical imaging of the developmental phases of human neuromelanin using synchrotron X-ray microspectroscopy. *Anal. Chem. 80*, 9557−9566.

(3) Szczerbowska-Boruchowska, M. (2008) X-ray fluorescence spectrometry, an analytical tool in neurochemical research. *X-Ray Spectrom. 37*, 21−31.

(4) Szczerbowska-Boruchowska, M., Stegowski, Z., Lankosz, M., Szpak, M., and Adamek, D. (2012) A synchrotron radiation micro-X-ray absorption near edge structure study of sulfur speciation in human brain tumors—A methodological approach. *J. Anal. At. Spectrom. 27*, 239−247.

(5) Bourassa, M. W., and Miller, L. M. (2012) Metal imaging in neurodegenerative diseases. *Metallomics 4*, 721−738.

(6) Chwiej, J., Dulinska, J., Janeczko, K., Appel, K., and Setkowicz, Z. (2012) Variations in elemental compositions of rat hippocampal formation between acute and latent phases of pilocarpine-induced epilepsy: An X-ray fluorescence microscopy study. *J. Bio. Inorg. Chem. 17*, 731−739.

(7) Chwiej, J., Kutorasinska, J., Janeczko, K., Gzielo-Jurek, K., Uram, L., Appel, K., Simon, R., and Setkowicz, Z. (2012) Progress of elemental anomalies of hippocampal formation in the pilocarpine model of temporal lobe epilepsy: An X-ray fluorescence microscopy study. *Anal. Bioanal. Chem. 404*, 3071−3080.

(8) Chwiej, J., Sarapata, A., Janeczko, K., Stegowski, Z., Appel, K., and Setkowicz, Z. (2011) X-ray fluorescence analysis of long-term changes in the levels and distributions of trace elements in the rat brain following mechanical injury. *J. Bio. Inorg. Chem. 16*, 275−283.

(9) Chwiej, J., Winiarski, W., Ciarach, M., Janeczko, K., Lankosz, M., Rickers, K., and Setkowicz, Z. (2008) The role of trace elements in the pathogenesis and progress of pilocarpine-induced epileptic seizures. *J. Biol. Inorg. Chem. 13*, 1267−1274.

(10) Hackett, M. J., Siegele, R., El-Assad, F., McQuillan, J. A., Aitken, J. B., Carter, E. A., Grau, G. E., Hunt, N. H., Cohen, D., and Lay, P. A. (2011) Investigation of the mouse cerebellum using STIM and μ-PIXE spectrometric and FTIR spectroscopic mapping and imaging. *Nucl. Instrum. Methods Phys. Res., Sect. B 269*, 2260−2263.

(11) Miller, L. M., Wang, Q., Telivala, T. P., Smith, R. J., Lanzirotti, A., and Miklossy, J. (2006) Synchrotron-based infrared and X-ray imaging shows focalized accumulation of Cu and Zn co-localized with beta-amyloid deposits in Alzheimer's disease. *J. Struct. Biol. 155*, 30−37.

(12) Popescu, B. F. G., George, M. J., Bergmann, U., Garachtchenko, A. V., Kelly, M. E., McCrea, R. P. E., Laning, K., Devon, R. M., George, G. N., and Hanson, A. D. (2009) Mapping metals in Parkinson's and normal brain using rapid-scanning x-ray fluorescence. *Phys. Med. Biol. 54*, 651.

(13) Popescu, B. F. G., Robinson, C. A., Chapman, L. D., and Nichol, H. (2009) Synchrotron X-ray fluorescence reveals abnormal metal distributions in brain and spinal cord in spinocerebellar ataxia: A case report. *Cerebellum 8*, 74−79.

(14) Popescu, B. F. G., Robinson, C. A., Rajput, A., Rajput, A. H., Harder, S. L., and Nichol, H. (2009) Iron, Copper and Zn distribution of the cerebellum. *Cerebellum 8*, 74−79.

(15) Pushie, M. J., Pickering, I. J., Martin, G. R., Tsutsui, S., Jirik, F. R., and George, G. N. (2011) Prion protein expression level alters regional copper, iron and zinc content in the mouse brain. *Metallomics 3*, 206−214.

(16) Leskovjan, A. C., Kretlow, A., Lanzirotti, A., Barrea, R., Vogt, S., and Miller, L. M. (2011) Increased brain iron coincides with early plaque formation in a mouse model of Alzheimer's disease. *NeuroImage 55*, 32−38.

(17) Leskovjan, A. C., Lanzirotti, A., and Miller, L. M. (2009) Amyloid plaques in PSAPP mice bind less metal than plaques in human Alzheimer's disease. *NeuroImage 47*, 1215−1220.

(18) Silasi, G., Klahr, A. C., Hackett, M. J., Auriat, A. M., Nichol, H., and Colbourne, F. (2012) Prolonged therapeutic hypothermia does not adversely impact neuroplasticity after global ischemia in rats. *J. Cereb. Blood Flow Metab. 32*, 1525−1534.

(19) Carmona, P., Rodriguez-Casado, A., Alvarez, I., de Miguel, E., and Toledano, A. (2008) FTIR Microspectroscopic Analysis of the Effects of Certain Drugs on Oxidative Stress and Brain Protein Structure. *Biopolymers 89*, 548−554.

(20) Chwiej, J., Dulinska, J., Janeczko, K., Dumas, P., Eichert, D., Dudala, J., and Setkowicz, Z. (2010) Synchrotron FTIR microspectroscopy study of the rat hippocampal formation after pilocarpine-evoked seizures. *J. Chem. Neuroanat. 40*, 140−147.
(21) Hackett, M. J., Borondics, F., Brown, D., Hirschmugl, C., Smith, S. E., Paterson, P. G., Nichol, H., Pickering, I. J., and George, G. N. (2013) A Sub-Cellular Biochemical Investigation of Purkinje Neurons Using Synchrotron Radiation Fourier Transform Infrared Spectroscopic Imaging with a Focal Plane Array Detector. *ACS Chem. Neurosci 4*, 1071−1080.
(22) Hackett, M. J., Lee, J., El-Assaad, F., McQuillan, J. A., Carter, E. A., Grau, G. E., Hunt, N. H., and Lay, P. A. (2012) FTIR Imaging of Brain Tissue Reveals Crystalline Creatine Deposits Are an *ex vivo* Marker of Localized Ischemia during Murine Cerebral Malaria: General Implications for Disease Neurochemistry. *ACS Chem. Neurosci. 3*, 1017−1024.
(23) Heraud, P., Caine, S., Campanale, N., Karnezis, T., McNaughton, D., Wood, B. R., Tobin, M. J., and Bernard, C. C. A. (2009) Early Dectection of the Chemical Changes Occurring During the Induction and Prevention of Autoimmune-mediated Demyelination Detected by FT-IR Imaging. *NeuroImage 49*, 1180−1189.
(24) Kastyak, M. Z., Szczerbowska-Boruchowska, M., Adamek, D., Tomik, B., Lankosz, M., and Gough, K. M. (2010) Pigmented creatine deposits in Amyotrophic Lateral Sclerosis central nervous system tissues identified by synchrotron Fourier Transform Infrared microspectroscopy and X-ray fluorescence spectromicroscopy. *Neuroscience 166*, 1119−1128.
(25) Kastyak-Ibrahim, M. Z., Nasse, M. J., Rak, M., Hirschmugl, C., Del Bigio, M. R., Albensi, B. C., and Gough, K. M. (2012) Biochemical label-free tissue imaging with subcellular-resolution synchrotron FTIR with focal plane array detector. *NeuroImage 60*, 376−383.
(26) Kneipp, J., Lasch, P., Baldauf, E., Beekes, M., and Naumann, D. (2000) Detection of pathological molecular alterations in scrapie-infected hamster brain by Fourier transform infrared (FT-IR) spectroscopy. *Biochim. Biophys. Acta, Mol. Basis Dis. 1501*, 189−199.
(27) Kneipp, J., Miller, L. M., Joncic, M., Kittel, M., Lasch, P., Beekes, M., and Naumann, D. (2003) *In situ* identification of protein structural changes in prion-infected tissue. *Biochim. Biophys. Acta, Mol. Basis Dis. 1639*, 152−158.
(28) Kretlow, A., Wang, Q., Kneipp, J., Lasch, P., Beekes, M., Miller, L., and Naumann, D. (2006) FTIR-microspectroscopy of prion-infected nervous tissue. *Biochim. Biophys. Acta, Biomembr. 1758*, 948−959.
(29) Kuzyk, A., Kastyak, M., Agrawal, V., Gallant, M., Sivakumar, G., Rak, M., Del Bigio, M. R., Westaway, D., Julian, R., and Gough, K. M. (2010) Association among amyloid plaque, lipid, and creatine in hippocampus of TgCRND8 mouse model for Alzheimer disease. *J. Biol. Chem. 285*, 31202−31207.
(30) Leskovjan, A. C., Kretlow, A., and Miller, L. M. (2010) Fourier Transform Infrared Imaging Showing Reduced Unsaturated Lipid Content in the Hippocampus of a Mouse Model of Alzheimer's Disease. *Anal. Chem. 82*, 2711−2716.
(31) Rodriguez-Casado, A., Alvarez, I., Toledano, A., de Miguel, E., and Carmona, P. (2007) Amphetamine effects on brain protein structure and oxidative stress as revealed by FTIR microspectroscopy. *Biopolymers 86*, 437−446.
(32) Hackett, M. J., McQuillan, J. A., El-Assaad, F., Aitken, J. B., Levina, A., Cohen, D. D., Siegele, R., Carter, E. A., Grau, G. E., Hunt, N. H., and Lay, P. A. (2011) Chemical alterations to murine brain tissue induced by formalin fixation: implications for biospectroscopic imaging and mapping studies of disease pathogenesis. *Analyst 136*, 2941−2952.
(33) Shivakumar, B. R., Kolluri, S. V. R., and Ravindranath, V. (1992) Glutathione homeostasis in brain during reperfusion following bilateral carotid artery occlusion in the rat. *Mol. Cell. Biochem. 111*, 125−129.
(34) Shivakumar, B. R., Kolluri, S. V. R., and Ravindranath, V. (1995) Glutathione and protein thiol homeostasis in brain during reperfusion after cerebral ischemia. *J. Pharmacol. Exp. Ther. 274*, 1167−1173.
(35) Winn, H. R., Rubio, R., and Berne, R. M. (1979) Brain adenosine production in the rat during 60 seconds of ischemia. *Circ. Res. 45*, 486−492.
(36) Veech, R. L., Harris, R. L., Veloso, D., and Veech, E. H. (1973) Freeze-blowing: A new technique for the study of brain in vivo. *J. Neurochem. 20*, 183−188.
(37) Folbergrova, J., Rehncrona, S., and Siesjo, B. K. (1979) Oxidized and reduced glutathione in the rat brain under normoxic and hypoxic conditions. *J. Neurochem. 32*, 1621−1627.
(38) Rehncrona, S., Folbergrova, J., Smith, D. S., and Siesjo, B. K. (1980) Influence of complete and pronounced incomplete cerebral ischemia and subsequent recirculation on cortical concentrations of oxidised and reduced glutathione in the rat. *J. Neurochem. 34*, 477−486.
(39) Cooper, A. J. L., Pulsinelli, W. A., and Duffy, T. E. (1980) Glutathione and ascorbate during ischemia and postischemic reperfusion in rat brain. *J. Neurochem. 35*, 1242−1245.
(40) Martin, H., and McIlwain, H. (1959) Glutathione, oxidised and reduced, in the brain and in isolated cerebral tissue. *Biochem. J. 71*, 275−280.
(41) Shank, R. P., and Aprison, M. H. (1971) Post-mortem changes in the content and specific radioactivity of several amino acids in four areas of the rat brain. *J. Neurobiol. 2*, 145−151.
(42) Lust, W. D., Passonneau, J. V., and Veech, R. L. (1973) Cyclic adenosine monophosphate, metabolites, and phosphorylase in neural tissue: A comparison of methods of fixation. *Science 181*, 280−282.
(43) Kneipp, J., Lasch, P., Baldauf, E., Beekes, M., and Naumann, D. (2000) Detection of pathological molecular alterations in scrapie-infected hamster brain by Fourier transform infrared (FT-IR) spectroscopy. *Biochim. Biophys. Acta, Mol. Basis Dis. 1501*, 189−199.
(44) Gallant, M., Rak, M., Szeghalmi, A., Del Bigio, M. R., Westaway, D., Yang, J., Julian, R., and Gough, K. M. (2006) Focally elevated creatine detected in amyloid precursor protein (APP) transgenic mice and alzheimer disease brain tissue. *J. Biol. Chem. 281*, 5−8.
(45) Dulinska, J., Setkowicz, Z., Janeczko, K., Sandt, C., Dumas, P., Uram, L., Gzielo-Jurek, K., and Chwiej, J. (2012) Synchrotron radiation Fourier-transform infrared and Raman microspectroscopy study showing an increased frequency of creatine inclusions in the rat hippocampal formation following pilocarpine-induced seizures. *Anal. Bioanal. Chem. 402*, 2267−2274.
(46) Pickering, I. J., Sneeden, E. Y., Prince, R. C., Block, E., Harris, H. H., Hirsch, G., and George, G. N. (2009) Localizing the Chemical Forms of Sulfur in vivo Using X-ray Fluorescence Spectroscopic Imaging: Application to Onion (Allium cepa) Tissues. *Biochemistry 48*, 6846−6853.
(47) Gnida, M., Yu Sneeden, E., Whitin, J. C., Prince, R. C., Pickering, I. J., Korbas, M. g., and George, G. N. (2007) Sulfur X-ray Absorption Spectroscopy of Living Mammalian Cells: An Enabling Tool for Sulfur Metabolomics. *In situ* Observation of Uptake of Taurine into MDCK Cells. *Biochemistry 46*, 14735−14741.
(48) Pickering, I. J., Prince, R. C., Divers, T., and George, G. N. (1998) Sulfur K-edge X-ray absorption spectroscopy for determining the chemical speciation of sulfur in biological systems. *FEBS Lett. 441*, 11−14.
(49) George, G. N., Pickering, I. J., Pushie, M. J., Nienaber, K., Hackett, M. J., Ascone, I., Hedman, B., Hodgson, K. O., Aitken, J. B., and Levina, A. (2012) X-ray-induced photo-chemistry and X-ray absorption spectroscopy of biological samples. *J. Synchrotron Rad. 19*, 875−886−0.
(50) Blusztajn, J. K., Zeisel, S. H., and Wurtman, R. J. (1979) Synthesis of lecithin (phosphatidylcholine) from phosphatidylethanolamine in bovine brain. *Brain Res. 179*, 319−327.
(51) Gharib, A., Sarda, N., Chabannes, B., Cronenberger, L., and Pacheco, H. (1982) The Regional Concentrations of S-Adenosyl-l-Methionine, S-Adenosyl-l-Homocysteine, and Adenosine in Rat Brain. *J. Neurochem. 38*, 810−815.
(52) Schatz, R. A., and Sellinger, O. Z. (1975) Effect of Methionine and Methionine Sulfoximine on Rat Brain S-adenosyl Methionine Level. *J. Neurochem. 24*, 63−66.

(53) Hoffman, D. R., Cornatzer, W. E., and Duerre, J. A. (1979) Relationship between tissue levels of S-adenosylmethionine, S-adenosylhomocysteine, and transmethylation reactions. *Can. J. Biochem. 57*, 56−64.
(54) Morrison, L. D., Smith, D. D., and Kish, S. J. (1996) Brain S-Adenosylmethionine Levels Are Severely Decreased in Alzheimer's Disease. *J. Neurochem. 67*, 1328−1331.
(55) Clarke, S., and Banfield, K. (2001) S-Adenosylmethionine-dependent methyltransferases. In *Homocysteine in health and disease* (Carmel, P., and Jaconbsen, D. W., Eds.), 1st ed., pp 63−78, Cambridge University Press, Cambridge.
(56) Araki, T., Kato, H., Inoue, T., and Kogure, K. (1990) Regional impairment of protein synthesis following brief cerebral ischemia in the gerbil. *Acta Neuropathol. 79*, 501−505.
(57) Matsui, Y., Kubo, Y., and Iwata, N. (1987) S-Adenosyl-L-methionine prevents ischemic neuronal death. *Eur. J. Pharmacol. 144*, 211−216.
(58) Lipton, P. (1999) Ischemic cell death in brain neurons. *Physiol. Rev. 79*, 1431−1568.
(59) Togawa, T., Ohsawa, A., Kawanabe, K., and Tanabe, S. (1997) Simultaneous determination of cysteine sulfinic acid and hypotaurine in rat tissues by column-switching high-performance liquid chromatography with electrochemical detection. *J. Chromatogr. B 704*, 83−88.
(60) Stitt, D. M., Kastyak-Ibrahim, M. Z., Liao, C. R., Morrison, J., Albensi, B. C., and Gough, K. M. (2012) Tissue acquisition and storage associated oxidation considerations for FTIR microspectroscopic imaging of polyunsaturated fatty acids. *Vib. Spectrosc. 60*, 16−22.
(61) Nasse, M. J., Walsh, M. J., Mattson, E. C., Reininger, R., Kajdacsy-Balla, A., Macias, V., Bhargava, R., and Hirschmugl, C. J. (2011) High-resolution Fourier-transform infrared chemical imaging with multiple synchrotron beams. *Nat. Methods 8*, 413−416.
(62) Zhang, J. Z., Bryce, N. S., Siegele, R., Carter, E. A., Paterson, D., de Jonge, M. D., Howard, D. L., Ryan, C. G., and Hambley, T. W. (2012) The use of spectroscopic imaging and mapping techniques in the characterisation and study of DLD-1 cell spheroid tumour models. *Integr. Biol. 4*, 1072−1080.
(63) Kutorasinska, J., Setkowicz, Z., Janeczko, K., Sandt, C., Dumas, P., and Chwiej, J. (2013) Differences in the hippocampal frequency of creatine inclusions between the acute and latent phases of pilocarpine model defined using synchrotron radiation-based FTIR microspectroscopy. *Anal. Bioanal. Chem. 405*, 7337−7345.
(64) Pickering, I. J., George, G. N., Yu, E. Y., Brune, D. C., Tuschak, C., Overmann, J., Beatty, J. T., and Prince, R. C. (2001) Analysis of Sulfur Biochemistry of Sulfur Bacteria using X-ray Absorption Spectroscopy. *Biochemistry 40*, 8138−8145.
(65) Sekiyama, H., Kosugi, N., Kuroda, H., and Ohta, T. (1986) *Bull. Chem. Soc. Jpn. 59*, 575−579.
(66) George, M. J. (2000) XAS-Collect: A computor program for X-ray absorption spectroscopic data acquisition. *J. Synchrotron Radiat. 7*, 283−286.
(67) George, G. N. http://ssrl.slac..stanford.edu/exafspak.html.